Cement & Concrete Composites 30 (2008) 566–575

Contents lists available at ScienceDirect

Cement & Concrete Composites

journal homepage: www.elsevier.com/locate/cemconcomp

The morphology of entrained air voids in hardened cement paste generated with different anionic surfactants

H.N. Atahan [a,*], C. Carlos Jr. [b], S. Chae [b], P.J.M. Monteiro [b], J. Bastacky [c]

[a] Istanbul Technical University, Civil Engineering Faculty, Structural Materials Department, Maslak, Istanbul, Turkey
[b] Department of Civil and Environmental Engineering, University of California-Berkeley, 721 Davis Hall, Berkeley, CA 94720, USA
[c] Children's Hospital Oakland Research Institute, 5700 Martin Luther King Jr. Way, Oakland, CA 94609, USA

ARTICLE INFO

Article history:
Received 15 January 2006
Received in revised form 5 December 2007
Accepted 22 February 2008
Available online 29 February 2008

Keywords:
Cement paste
Microstructure
Anionic surfactant
Entrained air
Air shell
ESEM
Surface tension
Foam index

ABSTRACT

The surface structures of entrained air voids in hardened cement paste were examined by means of an environmental scanning electron microscope (ESEM). Three different pure anionic surfactants were used: sodium dodecyl sulfonate (SDS), sodium dodecyl-benzene sulfonate (SDBS), and sodium oleate (SO). It was observed that a distinct shell forms around most of the entrained air voids regardless of the surfactant used. It was also shown that some hydration products can grow into the air voids at very early ages and may fill considerable amount of the void volume. In addition to the microscopic evaluation, a modified foam index test and surface tension measurements were also conducted on the solutions with different mixtures. It was determined that since oleate molecules coming from SO were precipitated in the mix as calcium oleate, exiguous amount of air bubbles were stabilized in the paste; however, when SDS and SDBS were used, an acceptable amount of air bubbles were stabilized.

1. Introduction

Concrete is the most widely used construction material throughout the world. However, this material is susceptible to deterioration from aggressive environmental conditions. The mostly widely seen deteriorations of concrete structures are sulfate attack, corrosion of steel reinforcement, freezing and thawing, and alkali silica reaction. The effects of such damage can impact both the domestic economy and global energy consumption.

Improvements in microscopy techniques have produced new insights to the microstructure of concrete giving new ideas and opportunities to understand the damage mechanisms of these detrimental effects. Many researchers have investigated freezing and thawing damage to concrete as early as the 1940s [1–5]. Since then, several mechanisms that damage concrete during freeze-thaw cycles of pore water have been identified: The hydraulic pressure [2] caused by the 9% volume increase as water undergoes a phase transformation into ice; the osmotic pressure [3] caused by the ion concentration difference between the frozen and the unfrozen parts of the connected pore system; and the thermodynamic disequilibrium [5–7] that occurs between the frozen and unfrozen parts which drives the super-cooled water towards the frozen sites to release its latent heat of fusion.

Regardless of the mechanisms that occur during freezing, escape surfaces are necessary to relieve the pressure in the cement matrix. Currently, air-entraining admixtures (AEAs) with different chemical compositions are widely used in the production of concrete in an attempt to extend its service life against the exposure to freeze-thaw cycles. AEAs belong to the group of chemical admixtures also known as "surfactants" which is an abbreviation of "surface active admixtures". Surfactants generally have a molecular structure of a long non-polar hydrocarbon chain and a polar group at one end [8]. Since surfactant molecules have a strong bipolar nature, they tend to be adsorbed and usually concentrate at the air-paste interface (i.e., around the air voids). As a result of this property, the surface layer around the entrained air voids may have a different composition with respect to the bulk fluid in the mixture. This should be taken into consideration regarding the morphology of air-paste interface zone.

Rashed and Williamson examined the microstructure of entrained air voids in concrete in 1991 [9,10]. In their study, the SEM micrographs (which were taken only 5 min after hydration) demonstrated the presence of very fine particles at the air void

* Corresponding author. Tel.: +90 (212) 285 3765.
E-mail addresses: hnatahan@ins.itu.edu.tr (H.N. Atahan), ccj@calmail.berkeley.edu (C. Carlos), busyrosy@berkeley.edu (S. Chae), monteiro@ce.berkeley.edu (P.J.M. Monteiro), jbastacky@chori.org (J. Bastacky).

0958-9465/$ - see front matter © 2008 Elsevier Ltd. All rights reserved.
doi:10.1016/j.cemconcomp.2008.02.003

shell. Thus, they concluded that the existence of these fine particles, which are mainly cement and silica fume (when added), explains the formation of the shells. A recent study by Corr [11,12] also observed the same thin shell forming at early hydration process when sodium oleate and sodium dodecyl-benzene sulfonate were used as surfactants. In addition, Corr also reported that the shell on the surface of the air void may prevent ice from penetrating into the air void, and increase the level of damage by generating extra hydraulic pressure inside the cement matrix. Consequently, studying the strength and the permeability of this shell will bring further insights to the damage mechanisms of freeze-thaw cycling.

The experimental work addressed in this paper examines the entrained air void surfaces using an 'environmental scanning electron microscope' (ESEM). Because the intention was to investigate the surface morphology of entrained air voids, fractured surface of specimens were not treated (e.g. carbon coating) to avoid damaging the surface. Three different pure surfactants were used with and without superplasticizer in order to observe the differences caused by these surfactants on the morphology of entrained air voids. In addition, modified foam index test and surface tension measurements were performed on the solutions containing surfactants to determine the surfactant-cement compatibility and to find out the performance of surfactants from the point view of their capability of reducing surface tension.

2. Materials

In this experimental work, the following three surfactants were used: sodium dodecyl sulfate (SDS), sodium dodecyl-benzene sulfonate (SDBS), and sodium oleate (SO). A polymerized naphthalene sulfonate (PNS) based superplasticizer was chosen because of its use in almost every commercial concrete mix. Six different mixes were examined as three surfactants were mixed with and without superplasticizer.

The major portion of commercial surfactants are based on relatively small amount of raw materials and these surfactants that are used in concrete technology are categorized into five different groups [13]: neutralized wood resins, fatty acid salts, alkyl–aryl sulfonates, alkyl sulfates, and phenol ethoxylates. SDS belongs to the alkyl sulfates group, SDBS belongs to the alkyl-aryl sulfates group, and SO belongs to the fatty acids salts group. A detailed classification and performance characteristics of air-entraining agents used in concrete technology can be found in [8]. ASTM C-150 type I/II cement was used and the water to cement ratio (w/c) of all mixes were kept constant at 0.35. The chemical composition of cement is given in Table 1. For all mixes, the amount of cement was kept constant at 50 g. All the pure surfactants were dissolved in the de-ionized water at a concentration of 0.5% (5 g surfactant per liter of water), or 0.18% of the weight of cement used, which may be considered to be high for a pure surfactant. When it was used, PNS was dissolved in the mixing water at a concentration of 1% (10 g PNS per liter of water), or 0.36% of the weight of cement used. Mixing sequence of the materials was as follows:

(1) Prepare surfactant solution.
(2) Incorporate superplasticizer to the surfactant solution when necessary.
(3) Add the solution into 50 g of cement and mix.

Table 1
Cement characteristics, mass%

Cement	K_2O	Na_2O	CaO (free)	C_3S	C_2S	C_3A	C_4AF
Type I/II	0.35	0.06	1.6	54.8	15.9	4.4	13.7

All the samples were prepared by hand-mixing vigorously for approximately 6–8 min and then by casting into $10 \times 10 \times 6$ mm plexiglass molds with a 1.5 mm deep notch inclusion. The notch in the sample guaranteed easy fracture and a leveled fractured surface.

3. Experimental methods

3.1. Foam index test

The purpose of the foam index test is to predict surfactant-cement compatibility using a simple method and evaluation. The modified foam index test proposed by Corr et al. [11] was deemed more applicable to this experiment because it allows a better comparison between the three surfactants with and without the effect of cement.

The procedure for the modified foam index test was as follows:

(1) Prepare 100 ml of surfactant–water solution 0.05 at% concentration (0.5 g surfactant per liter of water).
(2) Pour 20 ml of the surfactant–water solution into a 50 ml graduated cylinder. Add 4 g of cement when necessary ($w/c = 5$).
(3) Cap the graduated cylinder and shake continuously for 15 s. Record initial volume.
(4) Lay the cylinder on its side for 5 min.
(5) Record the final volume.

The absolute volume of the foam and the relative lack of change between the final and the initial volume of the foam indicate the foam stability. The compatibility between the cement and each surfactant can be implied by relative change in the foam stability between surfactant solution and surfactant solution with cement.

3.2. Surface tension tests

Surface tensions of the surfactants in different solutions were measured using the Wilhelmy Plate method [14]. The test method measures the force between a probe and the surface of a fluid. A rectangular roughened platinum thin section plate was used as a probe. The platinum plate was hung vertically on a balance and lowered until it came in contact with the solution surface. The plate was dipped 3 mm into the liquid, and raised up 1 mm. At the equilibrium point, the forces acting on the balance are the weight of the platinum plate, the up-thrust force on the submerged part of the plate, and the surface tension of the liquid touching the plate. The forces present in this situation are a function of the size and shape of the plate, the contact angle of the liquid/plate interaction, and the surface tension of the liquid. The contact angle of the liquid/plate interface is zero under the assumption that the solutions completely wet the plate. Consequently, the surface tension forces act directly downwards and in-plane on the platinum plate. The surface tension of the liquid is calculated by dividing the surface tension force (milliNewton, mN) to the wetted length of the plate (meter, m), which equals to two times the width of the Wilhelmy thin plate.

In our experiments, we used three pure surfactant solutions [Ss] with the same concentration used in the foam index test. In addition to the pure surfactant solutions, surface tensions measurements were also preformed on surfactant solutions suspended with portland cement [Ss + PC] and calcium hydroxide [Ss + CH]. The w/c ratio was kept constant at 5 and the calcium hydroxide saturated into solution as 0.16% by weight of the surfactant solution. Since suspended cement particles or dissolved $Ca(OH)_2$ particles influence the results, the samples were centrifuged to separate the particles from solution before testing. Furthermore, the

surfaces of the solutions were aspirated just before testing to remove floating particles and the thin film formed on the surfaces of the solutions. The laboratory temperature and relative humidity were 24 °C and 40%, respectively.

3.3. ESEM microscope

Typically micrographs are taken using scanning electron microscope (SEM) with high vacuum chambers. To obtain high range of magnification and clarity of images, the fractured surface had to be sanded smooth, dried, then carbon coated, which may alter the surface of the entrained voids. A Philips XL 30 Environmental Scanning Electron Microscope (ESEM) can produce micrographs of entrained air voids without the alterations to the fractured surface. ESEM is a very strong tool for the observation of cement paste at very early ages during hydration of cement when it is used in wet mode [15]. By the utilization of a cooling stage, the combination of low temperature (e.g. 4° C) and high water vapor pressure (e.g. 6.1 Torr) in the specimen chamber permits the user to achieve almost 100% relative humidity at the sample surface. In these conditions wet or hydrated specimens can be observed without drying in a natural environment.

For this experiment, a cooling stage was not available and specimens were observed at ambient temperature (approximately 20° C), pressure of about 2.3 torr, and relative humidity of 13% in the chamber. After casting, the samples were kept in a fog room until the evaluation day. Specimens were removed from the molds after 24 h, and were fractured moments before observation. Fractured surfaces of the specimens were examined at 1 and 7 days in the ESEM using a beam voltage of 10 kV and a working distance of around 10 mm. During the tests no charging was seen on the specimens' surface. Advantages of using ESEM are as follows:

(1) The specimens' fractured surfaces needed not undergo carbon coating surface treatments that would otherwise be required if conventional SEM was utilized.
(2) The ESEM made it possible to keep the pressure moderate in the specimen chamber (2.3 torr). A conventional SEM would require high vacuum (10^{-4}–10^{-9} torr) which may affect the surface properties.

4. Results and discussion

4.1. Foam index test

Fig. 1 presents a plot of the test results expressed in percent free volume of the graduated cylinder. Foam stability is implied by the lack of volume change 5 min after shaking. Evaluating the plot, all pure surfactant solutions showed no change in volume. Although SO solution produced less volume of foam, it still showed foam stability. The addition of cement decreased the initial volume of foam for all three surfactants. In addition, for the case of SDS and SBDS solution, the foam volume also decreased 5 min after shaking. The addition of cement for these two surfactants decreased the foam stability somewhat. In the case of SO, very little foam was produced after 15 s of shaking, suggesting that there was no foam stability and no likelihood of compatibility between the pure SO and the cement used.

4.2. Surface tension test

In order to understand the compatibility problem between sodium oleate and cement, surface tension measurements were taken on different solutions. Fig. 2 presents a plot of the surface tension test results. In this figure, the three groups of bars show surface tensions of SDS, SDBS, and SO solutions with different combinations such as cement and calcium hydroxide. The last bar shows the surface tensions of de-ionized water.

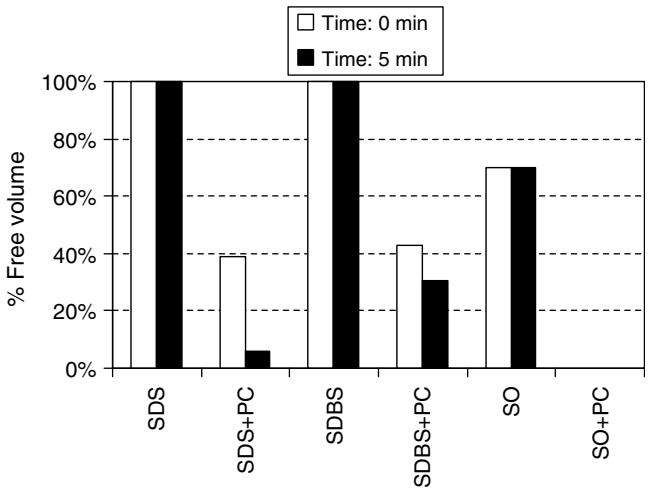

Fig. 1. Modified foam index test results.

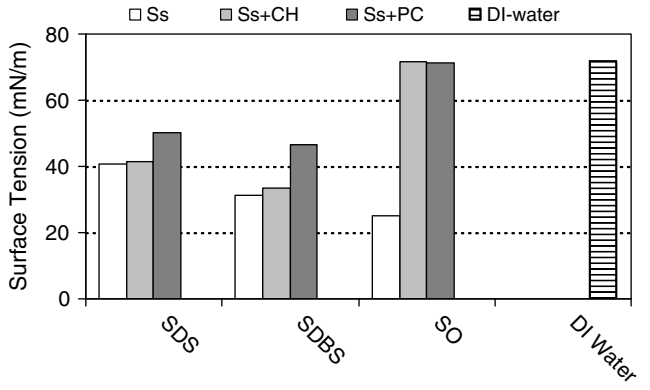

Fig. 2. Surface tension test results.

Comparing to the surface tension of de-ionized water measured as 71.7 mN/m, the surface tensions of surfactant solutions with SDS, SDBS, and SO were measured as 40.6, 31.1, and 25.2 mN/m, respectively. These initial results indicate a slightly greater reduction using SO in surface tension when compared to SDS and SDBS; however, when calcium hydroxide or Portland cement was included in the solutions, the surface tension of SO solution dramatically changed to values approximately equal to the surface tension of water. Similar results were experienced during the foam index test when the sodium oleate solution and cement were mixed.

Molecular formulas for this three anionic surfactants are as follows: SDS: $CH_3(CH_2)_{11}OSO_3Na$, SDBS: $CH_3(CH_2)_{11}C_6H_4SO_3Na$, and SO: $CH_3(CH_2)_7CH{=}CH(CH_2)_7COONa$. In solution, the surfactant molecules consist of a non-polar hydrocarbon chain with an anionic polar group. The anionic polar group of the SO consists of a carbon bonded with oxygen. The SDS and SDBS both have sulfate bonded with oxygen for their anionic polar group with SDBS including a benzene ring. Calcium ions bond with the anionic polar group forming most likely $CaSO_4$, $CaSO_4 \cdot 2H_2O$ and $CaCO_3$. The solubility's of $CaSO_4$, $CaSO_4 \cdot 2H_2O$ and $CaCO_3$ per 100 g of water are 0.209 g, 0.265 g and 1.5×10^{-3} g, respectively, [16]. The lower solubility of $CaCO_3$ indicates that it will remain as a precipitate rather than dissolve in water unlike the sulfate molecules, which will

more likely dissolve in water. When mixing solutions with cement or $Ca(OH)_2$, the calcium ions are released into the solution, and these ions react with the oleate forming calcium oleate [17], ($Ca(OL)_2$), which is an precipitant and almost insoluble in water. The solubility of calcium oleate per 100 g of water is $10^{-15.4}$ [17]. Since calcium ions have double positive charges, they need two oleate molecules when replacing with sodium ions: $(OL)-Ca^{2+}-(OL)$. Sodium oleate and Ca^{2+} ion interaction in the solution can be written as follows:

$$2[C_{17}H_{33}COO^{-}Na^{+}] + Ca^{2+} \rightarrow C_{17}H_{33}COO^{-}Ca^{2+-}OOCH_{33}C_{17} + 2Na^{+}.$$

From this equilibrium, it can be concluded that, the bond between the Ca^{2+} and the two polar heads of oleate molecules, COO^{-}, makes calcium oleate immiscible in water, which is similar to very low solubility of $CaCO_3$ in water. Consequently, precipitation of $Ca(OL)_2$ from solution prevents oleate molecules from generating and stabilizing foam. Basically, fatty acid salts like sodium oleate are considered 'soap'. Although soaps have similar molecular structures and properties as synthetic detergents like SDS and SDBS, they can easily react with ions of calcium to form $Ca(OL)_2$, where synthetic detergents do not react as readily with these ions. As a matter of fact, the problem here is similar to hard water, containing dissolved salts of calcium, magnesium and/or iron, and soap dissonance. The dissolved salts in hard water combine with soap molecules, and the resultant product is a water-insoluble scum, which is basically $Ca(OL)_2$. This phenomenon is also discussed by other researchers [18,19]. They explain that the air-entraining agent is precipitated by the calcium ions forming calcium salt, the surfactant then becomes unavailable for air-entraining action. However, the precipitants formed on the bubble surface may reinforce the air bubbles and prevent them from coalescence [18].

For the SDS solution, the addition of calcium hydroxide into the solution did not cause a remarkable change in surface tension and was measured as 41.6 mN/m. Portland cement added to SDS solution changed the surface tension from 40.6 to 50.0 mN/m, but this value is considerably below the surface tension of water and gives good results from the air entrainment point of view. The results for SDBS were very similar to SDS. Fore instance, calcium hydroxide included in solution with SDBS changed the surface tension from 31.1 to 33.6 mN/m, and for Portland cement changed to 46.4 mN/m. This value is also considered below the surface tension of water and as shown to work as air entrainment in cement pastes. Since SDS and SDBS are synthetic surfactants, they do not react as readily with calcium ions.

4.3. Microscopic evaluation

Since three different pure surfactants were used in this experimental work, this section of paper is broken into three parts: the results obtained from sodium dodecyl sulfate (SDS) mixes, the results obtained from sodium dodecyl-benzene sulfonate (SDBS) mixes, and the results obtained from sodium oleate (SO) mixes.

4.3.1. Sodium dodecyl sulfate (SDS) mixes

From the micrographs of 1 day old specimens, distinct shells around entrained air voids were observed when pure SDS was used with and without PNS. This agrees with the shell formation observed by Rashed et al. [9], who studied the early hydration of freeze dry cement paste samples with entrained air voids using a low temperature scanning electron microscope [20,21]. They note that the fine particles that make up the shell would react at a later age to form various hydration products.

According to the micrographs obtained in our work, the appearance of surface texture of voids with SDS specimens can be grouped into different categories depending on age and admixture combination. For 1 day old specimens, when PNS was not used, it was observed that some of the air voids have very smooth but perforated surfaces (Fig. 3a–c) while others had more crimpled surfaces (Fig. 3d). At the same time, some of the voids had many visible capillary openings on their surface while others had none. These phenomena are seen in Fig. 3a.

At 7-days, the same mix sample showed a change in surface characteristics of the entrained air voids. This was expected, since all the specimens were kept in a fog room for the duration of 7 days allowing the hydration process to continue. A number of voids

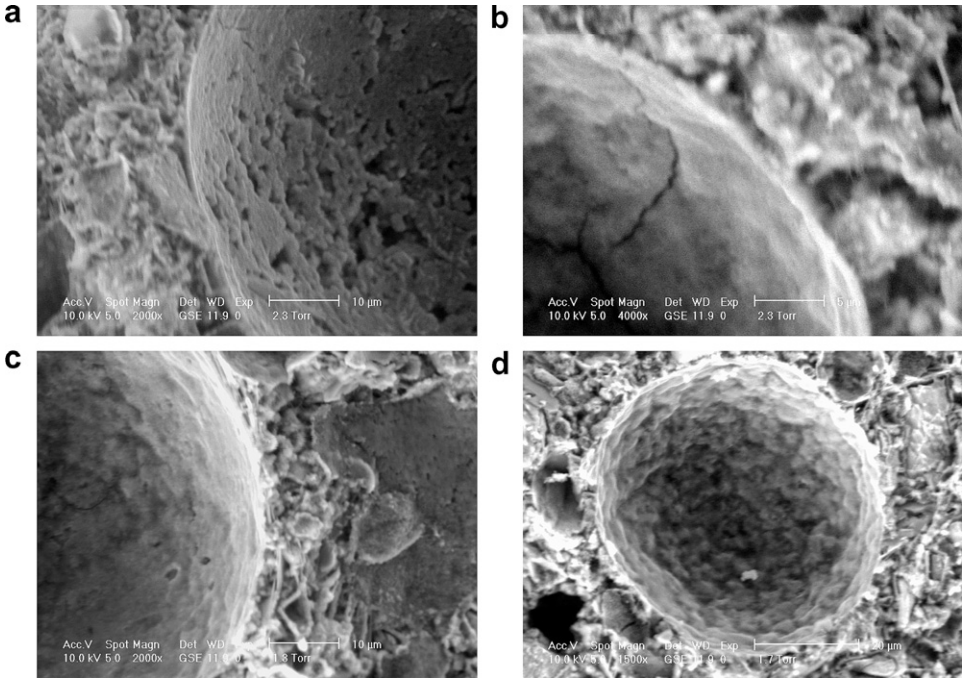

Fig. 3. Different voids from 1 day old SDS specimen without PNS.

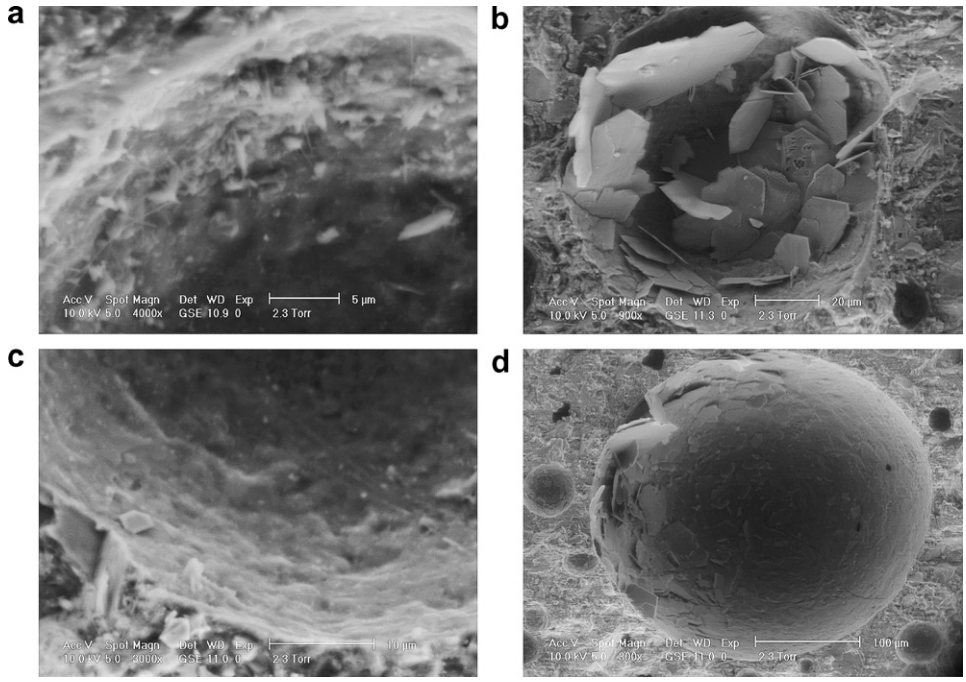

Fig. 4. Different voids from 7-day old SDS specimen without PNS.

were spotted with a growth of various hydration products (Fig. 4a and b). Especially apparent were slender and hexagonal shaped $Ca(OH)_2$ (CH) crystals. Sometimes, small needle-like crystals were observed in some of the voids (Fig. 4a). These crystals may either be ettringite or a form of calcium silicate hydrate. The appearance of the crystals may indicate an existence of water layer on the void surface during the hydration process. The thickness of the water layer on the surface may have a direct effect on the amount of these hydration products.

Another significant change between the surface characteristics of 1-day and 7-day specimen was the reduction in the visible capillary channel openings (Fig. 4c and d), leading the conclusions that the surface structure of entrained air voids get denser as cement hydration progresses. When the performance of air voids is taken into account, any change in the structure of the shell during hydration will have an effect on the frost durability of the cement based materials.

Since most of the capillary openings were filled or covered (Fig. 4c) by the hydration products, both physical and mechanical properties of air shell are affected. Decreased porosity of air shell will make the voids less permeable, causing an increase in hydraulic pressure in the matrix when the water freezes. If the expelled

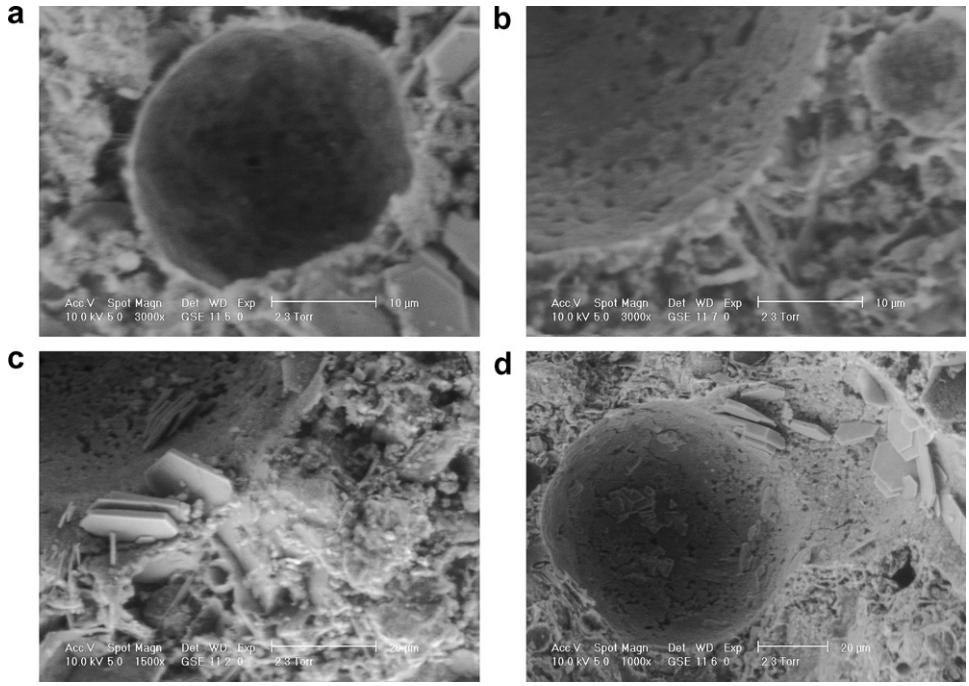

Fig. 5. Different voids from 1 day old SDS specimen with PNS.

water coming from freezing sites can penetrate into air voids without damaging the matrix, performance of air voids may not be affected. So, physical and mechanical properties of air shell should be studied further in detail to obtain more realistic modeling of ice damage mechanisms in cement based materials.

Excessive growth of hydration products within the entrained air voids may also reduce the air void performance during freeze-thaw cycles. As seen in Fig. 4b, the hydration products fill considerable amount of void volume, and significantly decrease the volume available for ice formation in the air void. It is also known that large crystals can form in the air voids when the concrete is kept under saturated conditions [22]. Since freeze-thaw cycles continually wet and dry the surface of the air voids, the hydration products can continue to grow inside air voids. Furthermore, the entrained air voids close to the surface may be more susceptible to this filling effect when spalling occurs. The total volume of entrained air voids may change during the service time of concrete structures depending on the conditions that the concrete is exposed.

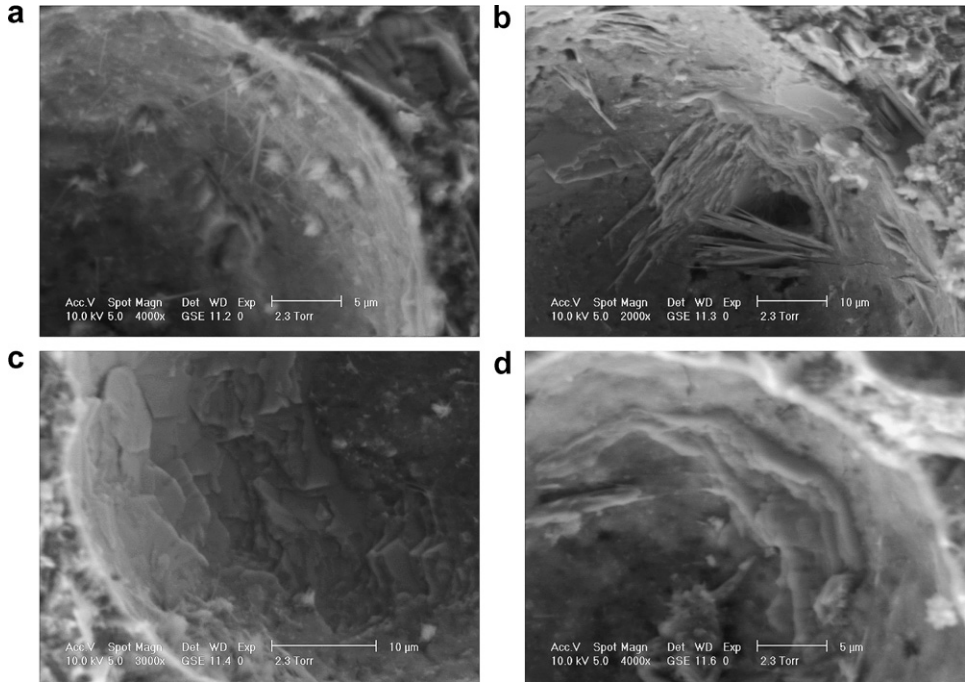

Fig. 6. Different voids from 7-day old SDS specimen with PNS.

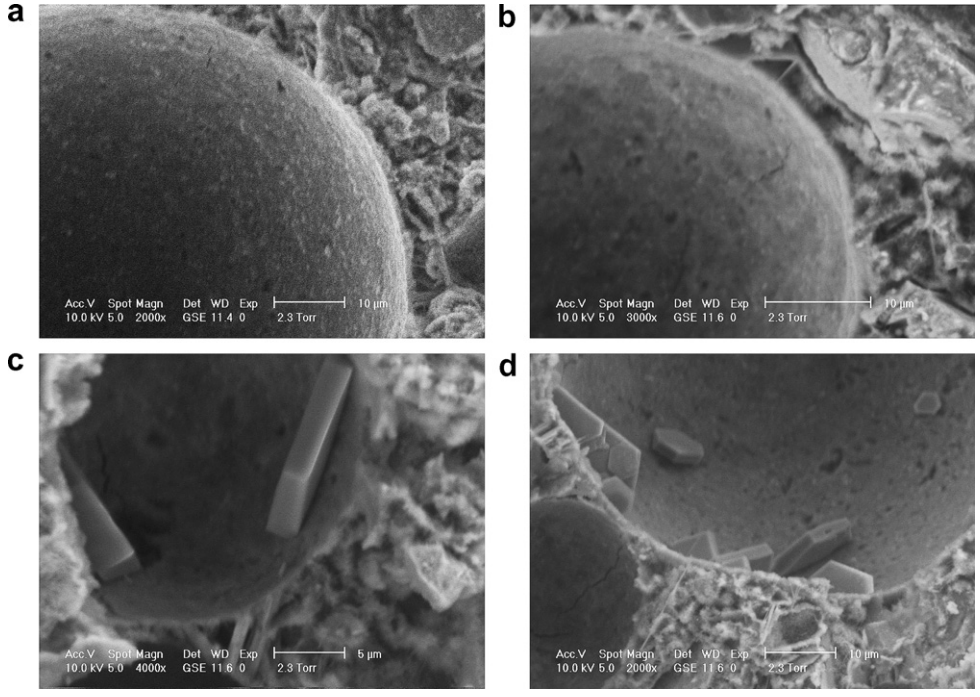

Fig. 7. Different voids from 1-day old SDBS specimen without PNS.

The micrographs of SDS samples with the combination of PNS have shown similar results as the samples without PNS. The voids also had smooth and perforated surfaces. For some of the voids, however, small quantities of CH crystal growth were observed in the 1-day specimen (Fig. 5a–d). This is contrary to what we saw in the specimen without PNS where no CH growth was observed after 1-day. The surface structure of the air voids in the 7-day specimen with PNS was also denser and covered with hydration products (Fig. 6a–d). Significant CH crystal growth was seen in both the samples with and without PNS which implies that PNS is not a contributing factor to CH growth.

4.3.2. Sodium dodecyl-benzene sulfonate (SDBS) mixes

Similar to the SDS specimens, distinct shells were seen around the entrained air voids when SDBS was used with and without PNS. Taking the 1-day old specimen without PNS into consideration, almost all of the entrained air voids had very smooth surfaces (Fig. 7a–d). On the surface of some of the voids, a few CH

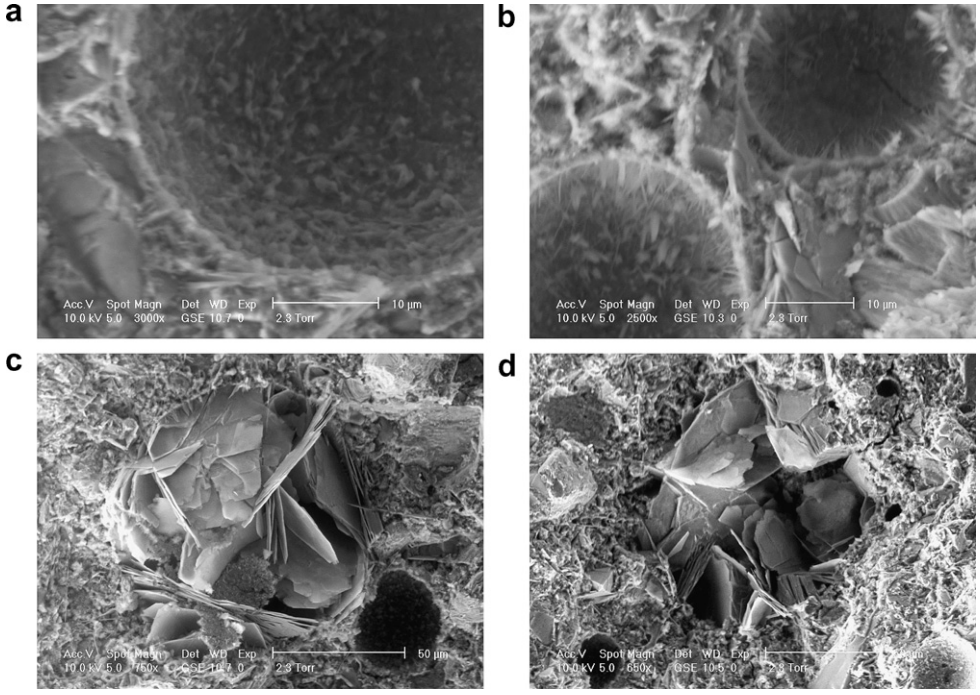

Fig. 8. Different voids from 7-day old SDBS specimen without PNS.

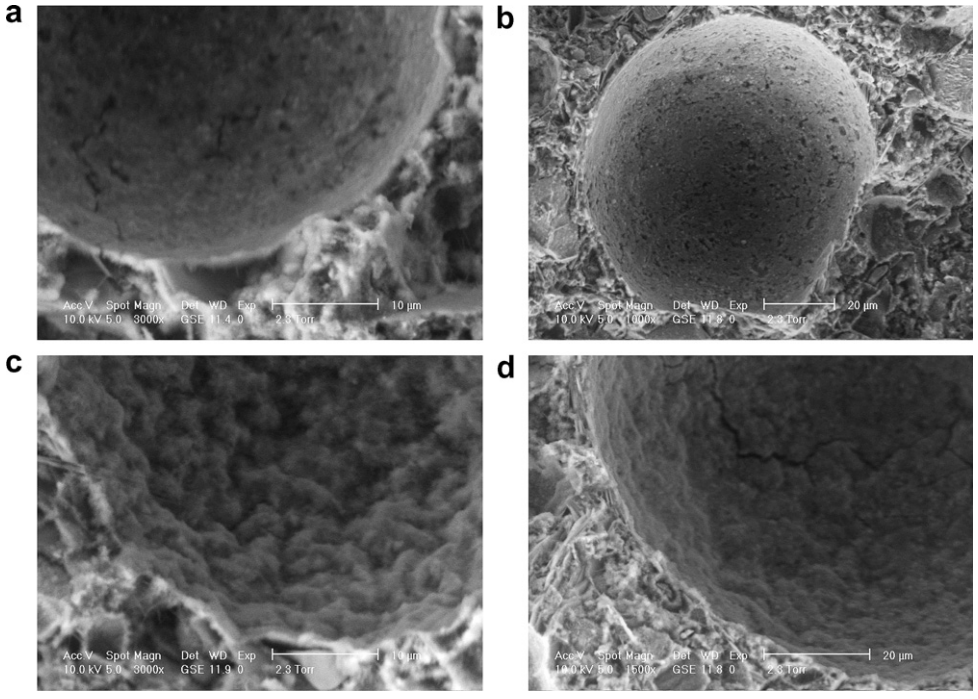

Fig. 9. Different voids from 1-day old SDBS specimen with PNS.

crystals were observed (Fig. 7c and d) at approximately 2 μm thickness. Capillary channel openings were also visible on the surface of 1-day specimen.

Micrographs of air voids from 7-day specimen without PNS are shown in Fig. 8. In respect to 1-day specimen (Fig. 7), it can be seen that the surface texture of air voids did not change dramatically. Almost all of the air voids observed in this specimen (Fig. 8a and b) showed very small needle-like crystal growth on their surfaces. To identify elemental composition of these crystals, a higher magnification range microscope with Energy dispersive X-ray spectroscopy (EDS) is necessary.

In Fig. 8c and d, two different air voids from the same sample is seen. These voids are almost filled by flaky and very thin hydration products. These thin crystals, although not distinctively hexagonal in shape, may be CH. Under ideal conditions of crystallization, CH crystals form as hexagonal plates. This shape was probably damaged during fracture process. On the other hand, it is also known that the growth pattern of CH can be altered by the admixtures used in the mix, especially affecting the aspect ratio of unit cell formed during cement paste hydration [23,24]. Berger and McGregor [23] have shown in their results that sulfates tend to produce CH morphology, reducing the aspect ration to below 0.5. Such phenomenon was observed on all of the CH crystals both in SDS and SDBS samples. Taylor [24] mentions that as the hydration proceeds, main deposits of CH become massive and indeterminate in shape with still good cleavage. This was observed in Fig. 8c and d, as opposed to perfectly shaped crystals that were seen in younger pastes (Fig. 5c and d).

In addition, most of the voids that were found filled with hydration crystals (Fig. 8c and d) were located very close to the specimen surface. Since all the specimens were kept in the fog room, condensation thus abundance of water on the surface of the specimen may contribute to relatively excessive crystal growth.

In Fig. 9a–d, some of the micrographs taken from the 1-day SDBS specimen with PNS are shown. According to these micrographs, the surface texture of the voids varied from smooth (Fig. 9a and b) to wrinkled (Fig. 9c and d). Note that the formation of distinct air shell is seen clearly on the boundaries of voids (Fig. 9a and c) regardless of void surface texture. In 1-day specimen, no hydration products were observed in the entrained air

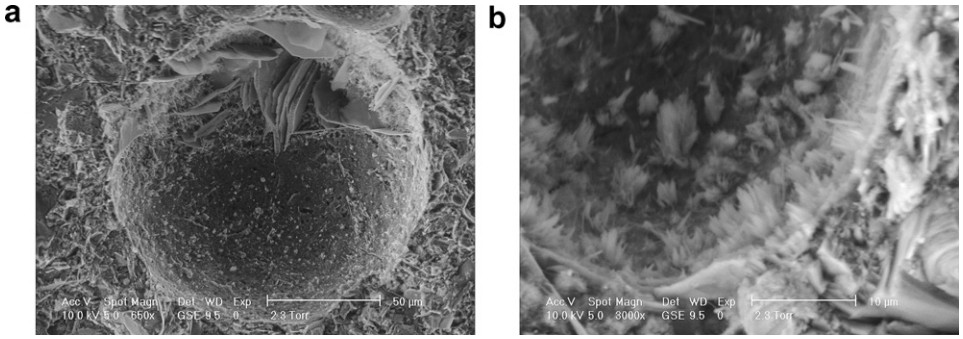

Fig. 10. Different voids from 7-day old SDBS specimen with PNS.

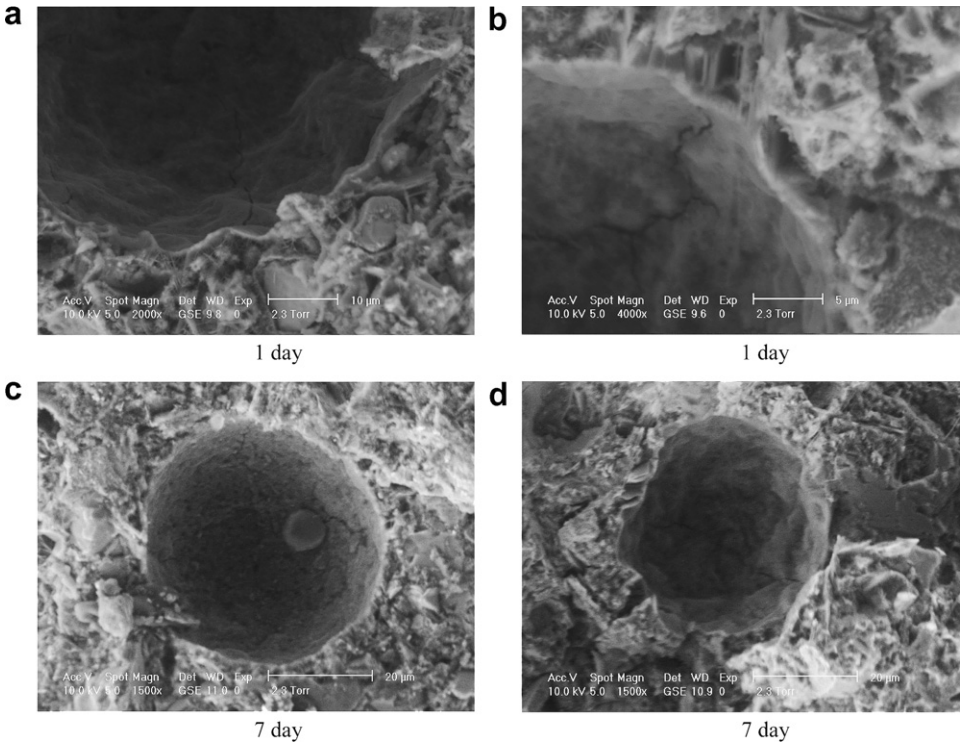

Fig. 11. Different voids from SO specimen without PNS.

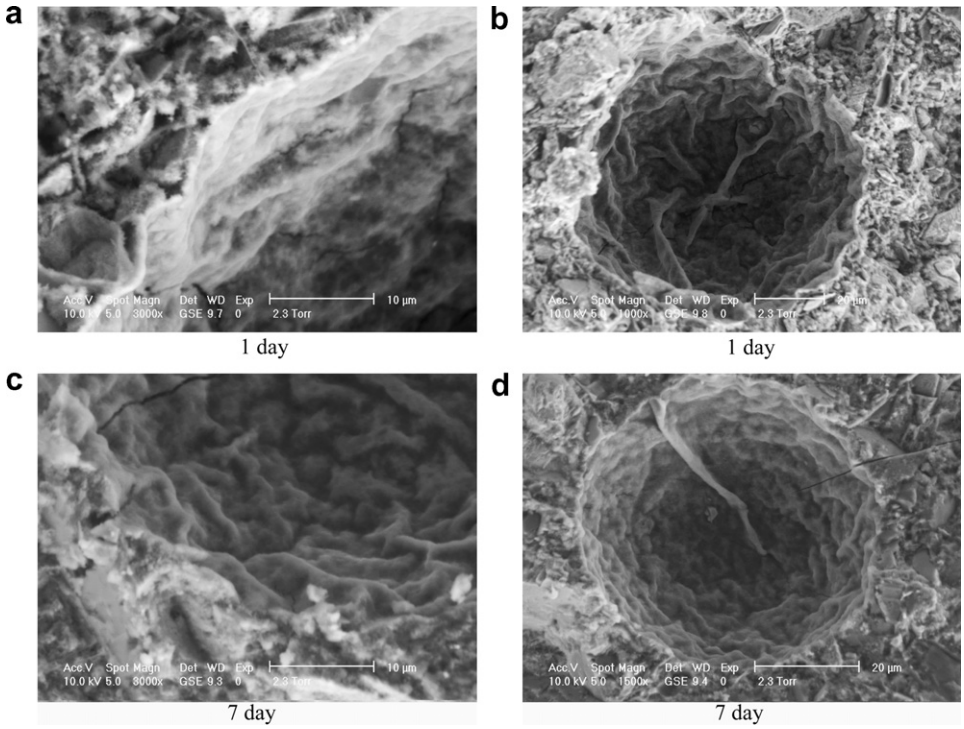

Fig. 12. Different voids from SO specimen with PNS.

voids. The 7-day specimen showed growth of flaky and needle-like crystal growth within the voids (Fig. 10a and b).

4.3.3. Sodium oleate (SO) mixes

The results of foam index test have shown that the combination of cement and SO caused very poor air entrainment in the cement matrix. This was also observed during the ESEM imaging on hardened cement paste samples. Comparing the SO with SDS and SDBS, there were significantly less entrained air voids in hardened cement pastes. The absence of voids also agreed with the surface tension measurements, which indicated a compatibility issue between the surfactant and the cement, more specifically, the calcium in the cement. The interactions between sodium oleate molecules and Ca^{2+} ions were discussed before. In brief, poor air entrainment was the result of precipitation of the oleate molecules in the mix and destruction of their air stabilizing properties. However, ESEM micrographs show that in spite of the precipitation of oleate molecules in the cement matrix, a small amount of entrained air voids were still observed with unusual surface structures (Figs. 11 and 12). In Fig. 11a–d, micrographs taken from 1 and 7-day old SO specimen without PNS are shown. Very little difference was observed over time. Most shell surfaces were wrinkly and very few channel openings were seen. There was no crystal growth observed in either specimen. Fig. 12a–d shows micrographs taken from 1 and 7-day old SO specimen with PNS. The difference between air voids with and without PNS is insignificant. All of the shells appeared to be wrinkled with no crystal growths for both 1 and 7-day old specimens. This structure may have been caused by precipitants of calcium oleate. Oleate molecules were adsorbed and concentrated on the air/water interface where they stabilized the air bubbles, but then were probably precipitated at the interface because of the calcium ions causing the wrinkled appearance. This appearance on the surface may also imply that these voids occupied larger space when they were being stabilized. To understand the exact composition of the surface, further analyses are required.

5. Conclusions

Within the limits of this experimental work, the results can be summarized as follows:

(1) A distinct shell forms around most of the entrained air voids regardless of the surfactant used. Physical and mechanical properties of this air shell may be affected from the type of surfactant used in the mixture.
(2) Hydration products, such as $Ca(OH)_2$ and needle-like crystals, grew into some of the air voids at very early ages. These products may fill a considerable amount of the void volume, which might affect the air void performance.
(3) Since a distinct shell forms around most of the entrained air voids, permeability properties of this shell should also be taken into consideration in the modeling of freezing of cementitious systems. However, further studies are needed to determine the permeability properties of this shell.
(4) Since oleate molecules were precipitated as calcium oleate when reacting with calcium in cement, exiguous amount of air bubbles were stabilized in the cement paste. However, when SDS and SDBS were used, acceptable amounts of entrained air voids was experienced in the cement paste.
(5) Within the limits of the materials used in this experimental work, it can be concluded that the surface characteristics of voids entrained with SDS and SDBS were too similar to separate the surface characteristics between SDS and SDBS voids. Because the surface structure of voids entrained by SO was unusual, it was excluded from this conclusion.
(6) The environmental scanning electron microscope can be used successfully as a strong tool for the observation of the microstructure of entrained air voids in cementitious systems.

Acknowledgements

The authors would like to recognize the National Science Foundation (NSF Grant 10143-23750-44) for their support of this research. The first author would like to recognize the Istanbul Technical University for their financial support during his stay in UC Berkeley. The authors would also like to thank Professor John A. Clements and Professor Jon Goerke of UC San Francisco for their assistance and discussions on surfactants, and Gordon Vrololjak of the Electron Microscope Laboratory (EML) for his assistance with the ESEM.

References

[1] Collins AR. The destruction of concrete by frost. J Inst Civil Eng 1944;23(1):29–41.
[2] Powers TC. A working hypothesis for further studies of frost resistance. J Am Conc Inst 1945;16(4):245–72.
[3] Powers TC, Helmuth RA. Theory of volume changes in hardened Portland cement pastes during freezing. Proc Highway Res Board 1953;32:285–97.
[4] Litvan GG. Frost action in cement paste. Mat Struct 1973;6(34):293–8.
[5] Everett DH. The thermodynamics of frost damage to porous solids. Trans Faraday Soc 1961;57:1541–51.
[6] Beaudoin JJ, MacInnis C. The mechanism of frost damage in hardened cement paste. Cem Conc Res 1974;4:139–47.
[7] Scherer GW. Crystallization of pores. Cem Conc Res 1999;29:1347–58.
[8] Whiting DA, Nagi MA. Manual on control of air content in concrete. Portland Cem Assoc 1998.
[9] Rashed AI, Williamson RB. Microstructure of entrained air voids in concrete: Part I. J Mater Res 1991;6(9):2004–12.
[10] Rashed AI, Williamson RB. Microstructure of entrained air voids in concrete: Part II. J Mater Res 1991;6(11):2074–83.
[11] Corr DJ, Monteiro PJM, Bastacky SJ, Gartner EM. Air void morphology in fresh pastes. Cem Conc Res 2002;32(7):1025–31.
[12] Corr DJ. A microscopic study of ice formation and propagation in concrete. PhD Thesis. Berkeley, University of California; 2001.
[13] Rixom R, Mailvaganam N. Chemical admixtures for concrete. New York: E&Spon; 1999.
[14] Hunter RJ. Introduction to modern colloid science. Oxford: Science Publications; 1994.
[15] Neubauer CM, Jennings HM. The role of environmental scanning electron microscope in the investigation of cement based materials. Scanning 1996;18:515–21.
[16] Hogness TR, Johnson WC, Armstrong AR. Qualitative analysis and chemical equilibrium. 5th ed. New York: Rinehart and Winston; 1996.
[17] Zhang H, Miller CA, Garrett PR, Raney KH. J Colloid Interf Sci 2004;279:539–47.
[18] Ramachandran VS. Concrete admixtures handbook: properties, science and technology. 2nd ed. Noyes Publications; 1995.
[19] Donson VH. Concrete admixtures. VNR Struc Eng Series. New York: Van Nostrand Reinhold; 1990.
[20] Bastacky J, Hook GR, Finch GL, Goerke J, Hayes TL. Low-temperature scanning electron microscope of frozen hydrated mouse lung. Scanning 1987;9:57–70.
[21] Corr DJ, Juenger MCG, Monteiro PJM, Bastacky J. Investigating entrained air voids and Portland cement hydration with low-temperature scanning electron microscope. Cem Conc Comp 2004;26:1007–12.
[22] Corr DJ, Monteiro PJM, Bastacky J. Microscopic characterization of ice morphology in entrained air voids. ACI Mater J 2002;99(2):190–5.
[23] Berger RL, McGregor JD. Influence of admixtures on the morphology of calcium hydroxide formed during tricalcium silicate hydration. Cem Conc Res 1972;2:43–55.
[24] Taylor HFW. Cem Chem. 2nd ed. Thomas Telfrod; 1997. p. 459.